Numerical Heat Transfer, Part A, 65: 949–971, 2014

ISSN: 1040-7782 print/1521-0634 online
DOI: 10.1080/10407782.2013.850971

Taylor & Francis
Taylor & Francis Group

A DIRECT NUMERICAL SIMULATION FOR NUCLEATE BOILING BY THE VOSET METHOD

Kong Ling, Zeng-Yao Li, and Wen-Quan Tao
Key Laboratory of Thermo-Fluid Science & Engineering, School of Energy & Power Engineering, Xi'an Jiaotong University, Xi'an, Shaanxi, P. R. China

This article presents a 2-D numerical simulation on nucleate boiling using the VOSET method. Heat transfer through a liquid microlayer around a three-phase contact point is incorporated by a multiscale system method. A temperature interpolation method is presented for solving temperature field in cells containing liquid-vapor interface. Apart from the single-bubble model, computations are carried out for two-bubble and bubble merger models. Heat fluxes predicted by simulation are compared with experimental correlations and good agreement is obtained. In addition, simulation results of bubble's behavior also verify some boiling mechanisms.

1. INTRODUCTION

Nucleate boiling is one of the most challenging problems for numerical simulation. This is because from a physical point of view phase change is a nano-scale phenomenon, and from an engineering point of view there are so many influencing factors on nucleate boiling heat transfer that until the 1990s we still did not know many things about boiling heat transfer, even at a phenomenological level [1]. In the past 25 years, researchers in the engineering heat transfer community, in conjunction with those thermal physicists, have made great progresses in further understanding and revealing the mechanism and behavior of nucleate boiling heat transfer. As far as a numerical approach is concerned, on one hand simulation methods at micro and meso scales have developed fast [2], which can help to reveal the basic features of the phase change processes. On the other hand, several engineering simulation models have been developed and successes have been obtained. These include the micro-convection model adopted in the RPI method [3], the numerical simulation of the bubble growing process [4], and the recently confirmed existence of liquid microlayer underneath a vapor bubble [5].

This article focuses on engineering simulation models. Broadly speaking, in all of the existing nucleate boiling heat transfer models, simulation starts from a bubble with a finite size, which bypasses the nucleation process and leaves it to the micro-level

Received 22 April 2013; accepted 13 September 2013.
Address correspondence to Wen-Quan Tao, Key Laboratory of Thermo-Fluid Science & Engineering, School of Energy and Power Engineering, Xi'an Jiaotong University, Xi'an, Shaanxi 710049, P. R. China. E-mail: wqtao@mail.xjtu.edu.cn

NOMENCLATURE

A	constant, (J)	v	velocity in y-direction
c	VOF function	x	coordinate
c_p	heat capacity	y	coordinate
$\vec{g}$	gravity acceleration, ($g = 9.8\,\mathrm{m/s^2}$)	β	thermal expansion coefficient
h	grid size	γ	latent heat of vaporization
H	Heaviside function	δ	liquid film thickness
L	wall length	κ	curvature
$\bar{m}$	mass flow rate	λ	thermal conductivity
$\dot{m}$	mass evaporation rate	μ	dynamic viscosity
M	total mass evaporation rate in micro region	ρ	density
		σ	surface tension coefficient
N	number of three-phase contact points	ϕ	signed distance function
p	pressure		
p_R	reference pressure	**Subscripts**	
q	average heat flux	l	liquid
q'	local heat flux	lv	liquid-vapor interface
t	time	*micro*	micro region
T	temperature	*macro*	macro region
$\vec{u}$	velocity vector	*sat*	saturation
u	velocity in x-direction	v	vapor
$\bar{u}$	average velocity	w	wall

study. In addition, all existing boiling heat transfer models adopt the concept that bubbles occur in ditches of the heat transfer surface [6, 7]. Then, according to the heat transfer governing equation in conjunction with interface capture techniques such as VOF [8], Level-Set [9], or their further developments such as VOSET [10], simulation can go on. The framework of such direct simulations of bubbles is principally the same, but in the practical implementations there are still quite a few different techniques and improvements that are needed. In the following, a brief review on some progresses in the direct simulation for nucleate boiling since 1999 will be presented.

By using the mesh-free numerical method, Yoon et al. [11] simulated the whole process of growing and departing a single bubble during nucleate boiling in two dimensions. In their study, the effect of microlayer is replaced by an initial superheated liquid layer around the interface.

Son et al. [4, 12] developed a microlayer model and performed numerical simulations on a single bubble evaporating from a horizontal surface in cylindrical coordinates. Liquid-vapor interface was captured by the Level-Set method. Good agreement with experimental results was obtained. Son and Dhir [13] simulated nucleate boiling on a horizon surface at high wall superheats in two dimensions and obtained good agreement (within $\pm 25\%$) with experimental correlation for the predicted heat flux.

Nam et al. [14] studied nucleate boiling on a superhydrophilic surface. In their numerical simulation, a very small contact angle ($<10^\circ$) was set for the capillary force on a solid surface.

Shin et al. [15] simulated nucleate boiling via level contour reconstruction method in three dimensions. The effect of nucleation site density was taken into

account by adjusting the size of computational domain. In their model, the microlayer evaporation was neglected and the bubble base (contact line on the heating wall) was assumed to keep still.

A more complete numerical simulation of nucleate boiling in three dimensions was performed by Mukherjee and Dhir [16]. They simulated the growing, merging, and departing of two and three bubbles that were initially set very close to each other. Interface was captured also by the Level-Set method and the effect of microlayer evaporation was taken into account by the model developed by Son et al. [4]. Based on these methods, Mukherjee and Kandlikar [17] simulated nucleate boiling of a single bubble with dynamic contact angle.

Aktinol and Dhir [18] carried out a numerical simulation on the thermal response of a solid surface during nucleate boiling of a single bubble. They also used the model of Son et al. [4] for microlayer evaporation.

It is an important feature of nucleate boiling that temperature in both liquid and vapor phases around the interface are varied along the normal to the interface. However, in most of the previous studies, temperature in the vapor phase is assumed constant and not solved during simulations. In addition, most of the numerical studies mentioned above adopted the Level-Set method to capture the interface. It is well-known that the Level-Set (LS) method has the weakness of loss/gain of mass [10]. Therefore, further improvement is needed to cope with such issues. The purposes of this study are to predict heat flux of nucleate boiling and analyze the mechanisms of the heat transfer by direct numerical simulation. In our model, the above-mentioned two problems are taken into consideration. The microlayer evaporation was incorporated using the model developed by Ma et al. [19]. The liquid-vapor interface is captured by VOSET developed by Sun and Tao [10], which possesses advantages and overcomes the disadvantages of both VOF and LS methods. Instead of assuming constant temperature in the vapor phase, a method for interpolating temperature in cells around interfaces is developed and the temperature field in both liquid and vapor phases is solved simultaneously. The simulations are carried out in two-dimensional Cartesian coordinates.

The outline of the article is organized as follows. In section 2, the micro-liquid layer model is first introduced, followed by its numerical solution. Numerical methods for the macro region are illustrated in section 3. Results are presented in section 4 where three examples, including single bubble rising, two bubbles rising and merging, are provided. Finally, some conclusions are made.

2. CONCEPT OF MICROLAYER AND ANALYSIS OF FLOW IN IT

As early as the 1950s it was suggested that growing bubble could trap a thin liquid layer, which could then evaporate and transfer large amounts of energy [5], and was further confirmed by the experiment of Cooper and Lloyd in 1969 [20]. To the authors' knowledge, it was Son et al. [4] who first incorporated this model into numerical simulation for bubble growing. They indicated that the liquid film thickness varies from the mesh size to the order of molecular size. As such, the computational domain is divided into macro and micro regions. Therefore, the simulation of bubble growing with the microlayer being taken into consideration is actually a multiscale problem [2]. Since for both the microlayer and the rest major part of

the computation domain governing equations based on the continuum assumption are applied, this is the so-called multiscale system problem [2]. As illustrated in Figure 1, the liquid film around a three-phase contact point is consists of an absorbed film region (region I), evaporating thin film (region II), and meniscus region (region III) [4]. Because of the adhesion of the solid surface, the liquid in region I does not evaporate even though it is superheated. Therefore, it can be treated as the superheated solid wall in simulation. The film thickness in this region is in order of molecular size. In region II, the film becomes thicker, the adhesion force becomes smaller and liquid can evaporate from the interface, but thickness of this region is still very thin, varying from order of molecular size to several micrometers. Since the thickness of the major part of this layer is much smaller than a cell's size in the macro region, heat transfer and evaporation in region II should be solved separately. Region III can be treated as part of the macro region, for the film is thick enough.

Based on the above understanding, a detailed mathematical model for predicting heat transfer through the microlayer in two dimensions was developed by Ma et al. [19]. In their model, the flow in the microlayer is assumed to be steady and solved by the Navier-Stocks equation. It was found by Ma et al. that the effect of the advection term is small and can be neglected. Thus, the momentum equation can be simplified as follows:

$$-\frac{\partial p}{\partial x}+\mu_l\left(\frac{\partial^2 u}{\partial x^2}+\frac{\partial^2 u}{\partial y^2}\right)=0 \tag{1}$$

The pressure in the micro liquid film is calculated by the following equation.

$$p=p_R-\frac{A}{\delta^3}-\kappa\sigma \tag{2}$$

in which p_R is the reference pressure assumed to be constant, A is a constant equal to 10^{-20} J, δ is the film thickness, σ is the surface tension coefficient, κ is the interface

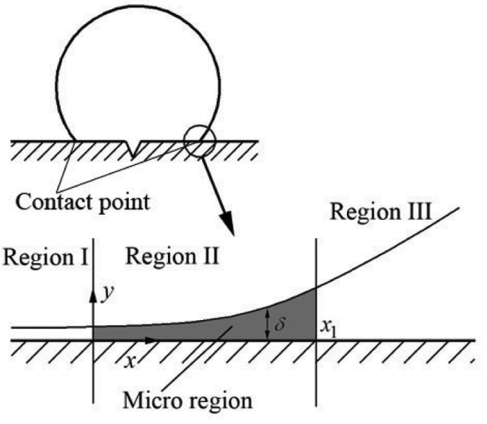

Figure 1. Micro region in computational domain.

curvature, and it is related to δ as follows

$$\kappa = \frac{\delta_{xx}}{\left(1+\delta_x^2\right)^{3/2}} \tag{3}$$

where δ_x, δ_{xx} are the first order and second order derivatives of δ with respect to x. The momentum equation is integrated in y-direction from 0 to δ and u is assumed to be parabolic. It can be reduced to the following.

$$-\frac{3A}{\delta^4}\frac{d\delta}{dx}\delta + \sigma\frac{d\kappa}{dx}\delta + \mu_l\frac{d^2(\bar{u}\delta)}{dx^2} = \mu_l\left.\frac{\partial u}{\partial y}\right|_0^\delta = \frac{3\mu_l\bar{u}}{\delta} \tag{4}$$

In which $\bar{u}$ is the average velocity, $\bar{u} = -\int_0^\delta u dy$.

The mass flow rate is defined by the following.

$$\bar{m} = \rho_l\delta\bar{u} \tag{5}$$

It can be related to evaporation on the interface caused by heat transfer through the liquid film as follows.

$$\frac{d\bar{m}}{dx} = \frac{q'}{\gamma} = \frac{\lambda_l(T_w - T_{lv})}{\gamma\delta} \tag{6}$$

where q' denotes local heat flux, it is computed by heat conduction through the liquid film. T_{lv} represents temperature of liquid-vapor interface on the top of the liquid film. It can be determined by using the Clausius-Clapyron equation.

$$T_{lv} = T_v\left(1+\frac{\Delta p}{\rho_v\gamma}\right) \tag{7}$$

where $\Delta p = \frac{A}{\delta^3} + \kappa\sigma$ and the temperature should be computed in Kelvin degree.

Combining Eqs. (4) and (6), the momentum equation becomes the following.

$$\frac{d}{dx}\left(-\left(\frac{3A}{2\delta^3}+\sigma\kappa\right)\delta + \frac{\mu_l\lambda_l(T_w - T_{lv})}{\rho_l\gamma\delta}\right) = \frac{3\mu_l\bar{m}}{\rho_l\delta^2} - \sigma\kappa\frac{d\delta}{dx} \tag{8}$$

By defining intermediate variables $F = -\left(\frac{3A}{2\delta^3}+\sigma\kappa\right)\delta + \frac{\mu_l\lambda_l(T_w-T_{lv})}{\rho_l\gamma\delta}$ and $G = \frac{d\delta}{dx}$, the problem can be described by five first-order ordinary differential equations (6) and (9)–(12).

$$\frac{dF}{dx} = \frac{3\mu_l\bar{m}}{\rho_l\delta^2} - \sigma\kappa G \tag{9}$$

$$\frac{d\bar{u}}{dx} = \frac{\lambda_l(T_w - T_{lv})}{\gamma\rho_l\delta^2} - \frac{\bar{u}}{\delta}G \tag{10}$$

$$\frac{dG}{dx} = \kappa\left(1 + G^2\right)^{3/2} \tag{11}$$

$$\frac{d\delta}{dx} = G \tag{12}$$

In the numerical solution of this problem, the five variables $\bar{m}_n$, F_n, $\bar{u_n}$, G_n, and δ_n at node x_n can be solved by values at x_{n-1}. The other two variables κ_n and $T_{lv,n}$ can be solved by combining Eq. (7) and the definition of F. The calculation should be started at the junction of regions I and II ($x = 0$) and should be ended at the junction of regions II and III ($x = x_1$), where the disjoining pressure (A/δ^3) is small enough, i.e., less than 0.01 Pa. For more details about this model, please refer to reference [19].

In numerical simulation for the examples of this study the properties of water at atmosphere are used. The wall temperature superheat is 7 K, so $T_v = 373.15$ K and $T_w = 380.15$ K. The properties of liquid and vapor phases are listed in Table 1.

Figures 2–4 illustrate the variations of the film thickness, interface temperature, and heat flux, respectively, with x in the micro region solved by the above model. The disjoining pressure at the right boundary is 0.005 Pa, the corresponding film thickness is 1.71 μm. At left boundary the liquid-vapor interface temperature is equal to wall temperature. Hence, no heat transfer occurs at this point because of zero temperature difference. As the location just departs from this point, the interface temperature decreases rapidly while the film is still very thin. Thus the local heat flux increases significantly and reaches a peak of very high value (about 7×10^7 W/m^2). Then because of the rapid decrease in the interface temperature and the increase in the film thickness with x, the local heat transfer flux decreases dramatically. As the location gets closer to the macro region, the decrease of the local heat flux becomes mild and the local heat flux gradually approaches zero because the local interface temperature is close to the saturated temperature.

For every contact point, the total mass evaporation rate caused by heat transfer through the microlayer can be computed by integrating the heat flux along the domain of the micro region.

$$M = \frac{1}{\gamma}\int_0^{x_1} q' dx \tag{13}$$

It will be used in computation of the macro region.

Table 1. Properties of liquid and vapor phases

	Liquid	Vapor
Density (kg/m^3)	958	0.6
Dynamic viscosity (kg/(m · s))	2.82×10^{-4}	12.3×10^{-6}
Thermal conductivity (W/(m · K))	0.683	0.025
Thermal capacity (J/(kg · K))	4220	2100
Latent heat (J/kg)	2,257,000	
Surface tension coefficient (N/m)	0.059	

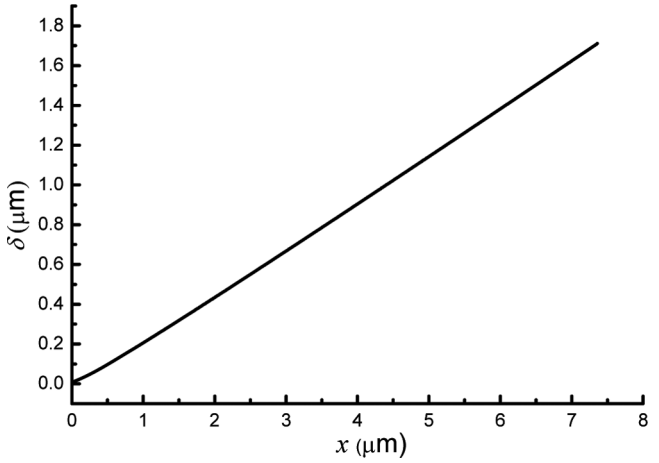

Figure 2. Film thickness in micro region.

The heat flux through the microlayer can be averaged over the wall

$$q_{micro} = \frac{N}{L} \int_0^{x_1} q' dx \tag{14}$$

in which N denotes the number of three-phase contact points, and L denotes the wall length in the whole computational domain.

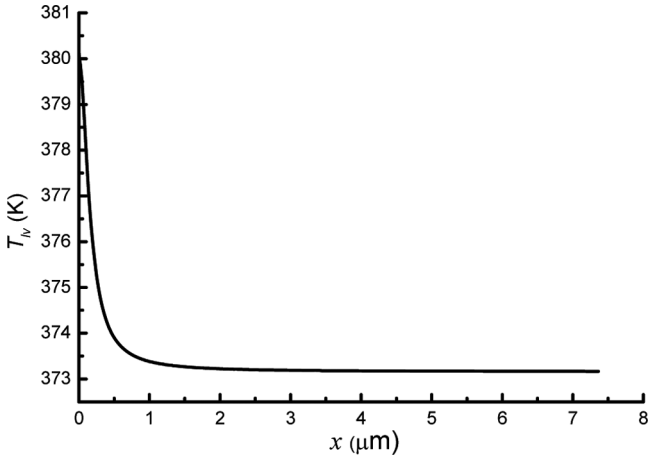

Figure 3. Interface temperature variation in micro region.

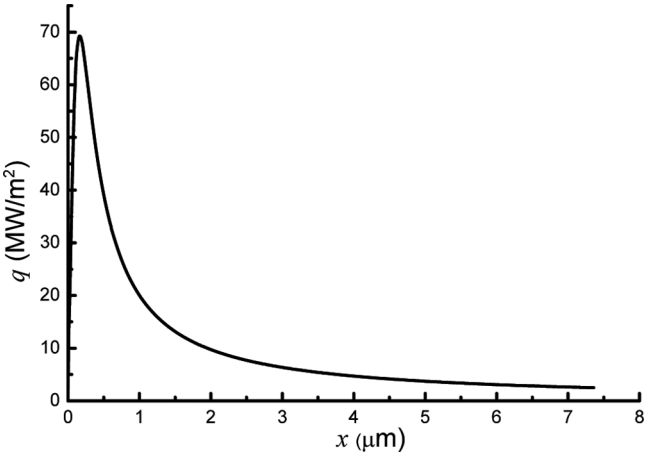

Figure 4. Local heat flux in micro region.

3. NUMERICAL SOLUTION FOR MACRO REGION

3.1. Governing Equation

The Navier-Stocks equation and continuity equation are solved for both liquid and vapor phases. For the two-phase flow without phase change following equation holds

$$\rho\left(\frac{\partial \vec{u}}{\partial t} + (\vec{u}\cdot\nabla)\,\vec{u}\right) = -\nabla p + \nabla\cdot\left(\mu\nabla\vec{u} + \mu\nabla\vec{u}^{T}\right) + \rho\vec{g} - \mathrm{H}\rho\beta_T(T - T_{sat})\vec{g} + \sigma\kappa\nabla\mathrm{H} \tag{15}$$

$$\nabla\cdot\vec{u} = 0 \tag{16}$$

$$\frac{\partial c}{\partial t} + \vec{u}\cdot\nabla c = 0 \tag{17}$$

where c is VOF function with its value varying from 0 to 1. But for the present study in the cells containing liquid-vapor interfaces heat transfer occurs with some liquid being evaporated, some modifications should be added for taking into account of vaporizing. The new governing equation of VOF is preseuted as follows.

The equations should be derived from the universal continuity equation.

$$\frac{\partial \rho}{\partial t} + \nabla\cdot(\rho\vec{u}) = 0 \tag{18}$$

By the definition of VOF function:

$$\rho = c\rho_v + (1 - c)\rho_l \tag{19}$$

Substitute Eqs. (19) into (18), it yields the following equation,

$$\frac{\partial c}{\partial t} + \nabla \cdot (c\vec{u}) = \frac{\rho_l}{\rho_l - \rho_v} \nabla \cdot \vec{u} \tag{20}$$

The velocity divergence contained in Eq. (20) is caused by volume expansion owing to mass evaporation. It can be computed by the following

$$\nabla \cdot \vec{u} = (\dot{m}_{macro} + \dot{m}_{micro}) \left(\frac{1}{\rho_v} - \frac{1}{\rho_l} \right) \tag{21}$$

in which $\dot{m}_{micro}$ and $\dot{m}_{macro}$ represent the mass evaporation rate caused by heat transfer in the micro and macro regions, respectively. $\dot{m}_{micro}$ is computed by the total mass evaporating rate M (Eq. (13)) solved in microlayer by the assumption that the mass evaporation rate in the microlayer around a three-phase contact point is shared averagely by the whole bubble interface that contains this contact point. $\dot{m}_{macro}$ can be computed along with solving the energy equation, which will be discussed below.

Consider a volume V fixed in space, Γ is the liquid-vapor interface inside V. $\dot{m}_{macro}$ is related to the heat that the interface gains.

$$\int_V \dot{m}_{macro} dV = \frac{1}{\gamma} \int_\Gamma \dot{q} dS \tag{22}$$

The interface gains heat from both phases [22].

$$\dot{q} = \lambda_v \left. \frac{\partial T}{\partial n} \right|_v - \lambda_l \left. \frac{\partial T}{\partial n} \right|_l \tag{23}$$

in which n denotes the interface normal pointing from liquid to vapor phase.

In Eq. (23), it can be seen that to obtain the interface heat flux temperature distributions in both liquid and vapor are needed, which can be obtained by solving the energy equation. The energy equation can be written as follows.

$$\frac{\partial (\rho c_p T)}{\partial t} + \nabla \cdot (\rho c_p \vec{u} T) = \nabla \cdot (\lambda \nabla T) \tag{24}$$

It should be noted, that the above equation is solved in cells occupied by liquid or vapor phase that contains no interface. Since vaporizing occurs only on the interface, no source term should be added in the energy equation for pure liquid and vapor. For the cells that contain interface, the energy equation is not solved and temperature is obtained by interpolating with the condition that $T = T_{sat}$ on the interface.

3.2. Interface Capture

In the present study, the volume-of-fluid Level-Set (VOSET) method [10] that combines both advantages of VOF and Level-Set is used for interface capturing. In

the VOSET method, VOF function c is solved first, and then signed distance function ϕ is solved by VOF function. In this study, $c=1$ and the negative sign of ϕ refer to vapor phase; Youngs-PLIC is used to solve VOF function. The signed distance function is used to compute the smoothed Heaviside function $H(\phi)$.

$$H(\phi)=\begin{cases}0 & \text{for } \phi<-\varepsilon\\ \frac{1}{2}\left(1+\frac{\phi}{\varepsilon}-\frac{1}{\pi}\sin\frac{\pi\phi}{\varepsilon}\right) & \text{for}|\phi|\le\varepsilon\\ 1 & \text{for } \phi>\varepsilon\end{cases} \tag{25}$$

where ε denotes the width of transition region for smoothing.

The smoothed density and viscosity in momentum equation are computed by the following.

$$\rho=\rho_l H(\phi)+\rho_v(1-H(\phi)) \tag{26}$$

$$\mu=\mu_l H(\phi)+\mu_v(1-H(\phi)) \tag{27}$$

For more details about VOSET, please refer to reference [10].

In the following presentation, numerical solutions of the governing equations will be described. Since the solution of energy equation involves much more technical details, for the convenience of presentation the solution methods of the two equations are separately presented.

3.3. Numerical Solution of Momentum Equation

The momentum equation is discretisized by finite volume method [20, 21] in staggered grid. QUICK [21] is used for the discretization of the advection term and central difference scheme is used for the diffusion term. Surface tension is computed as a source term of momentum equation by CSF model [23]; Interface curvature is computed by height function (HF) method [22]. Contact angle is taken into account also by HF method [24]. In this study, contact angle is assumed to be constant and equal to 45°. Projection method [22] is used for solving pressure and velocity field.

3.4. Numerical Solution of Energy Equation

As mentioned above, the energy equation is solved only for single phase, either liquid or vapor. Cells in the whole computational domain can be divided into two types. The first type contains a piece of interface, where $0<c<1$, and the second type contains no interface. It is evident that vaporization occurs only in the cells of the first type. Thus, the temperature in the cells of the second type is solved by Eq. (24). In the discretization of the energy equation, MUSCL [25, 26] is used for the advection term and CD is used for the diffusion term. For cells of the first type, the temperature should be interpolated. Guo et al. developed a method for interpolating temperature in the vapor phase in simulation of film boiling [27, 28]. Here, this method is expanded to interpolate temperature of both liquid and vapor phase around the interface.

Consider cell (i, j) of the first type. It should be known a priori which phase the center of the cell is located in, and this can be determined by the sign of $\phi_{i,j}$. If $\phi_{i,j}$ is

positive, its center is located in liquid phase and $T_{i,j}$ should be interpolated by neighboring cells whose centers are also located in liquid phase, as shown in Figure 5.

The temperature gradient in the liquid side can be estimated by the following.

$$\frac{\partial T}{\partial n} = \nabla T \cdot \vec{n} \approx \frac{T_{i+1,j} - T_{i,j}}{H_x} |n_x| + \frac{T_{i,j-1} - T_{i,j}}{H_y} |n_y| \tag{28}$$

It also can be estimated by the following.

$$\frac{\partial T}{\partial n} \approx \frac{T_{i,j} - T_{sat}}{D} \tag{29}$$

in which $D = |\phi_{i,j}|$.

Thus, $T_{i,j}$ can be estimated by: $\frac{T_{i,j}-T_{sat}}{D} = \frac{T_{i+1,j}-T_{i,j}}{H_x}|n_x| + \frac{T_{i,j-1}-T_{i,j}}{H_y}|n_y|$, and it yields,

$$T_{i,j} \approx \frac{A}{B} \tag{30}$$

in which,

$$A = D\left(\frac{|n_x|}{H_x} T_{i+1,j} + \frac{|n_y|}{H_y} T_{i,j-1}\right) + T_{sat} \tag{31a}$$

$$B = D\left(\frac{|n_x|}{H_x} + \frac{|n_y|}{H_y}\right) + 1 \tag{31b}$$

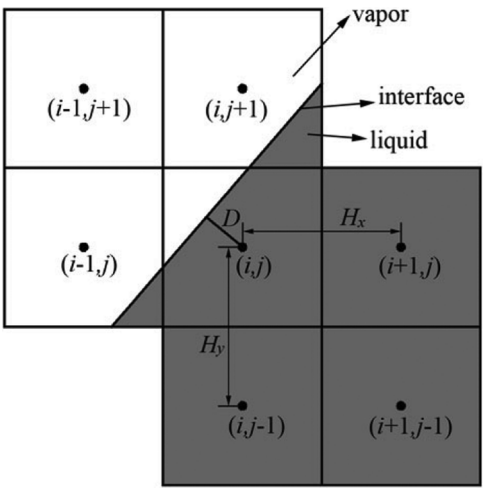

Figure 5. Illustration of temperature interpolation method.

If $\phi_{i,j} < 0$, the center of cell (i, j) is located in the vapor phase; for this case,

$$A = D\left(\frac{|n_x|}{H_x} T_{i-1,j} + \frac{|n_y|}{H_y} T_{i,j+1}\right) + T_{sat} \tag{31c}$$

while other expressions are the same.

In this temperature interpolation process for the cells containing interfaces, the temperature gradient on one side (denoted as $\left(\frac{\partial T}{\partial n}\right)_1$) can be obtained which will be used in Eq. (23). Meanwhile, the temperature gradient on the other side (denoted as $\left(\frac{\partial T}{\partial n}\right)_2$) is also needed. When (i,j) is in the liquid side, the derivative takes subscript 1 and the other one takes v, and vice versa. Actually, for distance function is computed before, the temperature gradient on the other side can be estimated by any of the three neighboring cells (points A–C shown in Figure 6). For better accuracy, a proper cell is chosen according to the interface direction.

$$\left(\frac{\partial T}{\partial n}\right)_2 \approx \begin{cases} \frac{T_A - T_{sat}}{|\phi_A|} & \text{if } \theta \le 30^\circ \\ \frac{T_B - T_{sat}}{|\phi_B|} & \text{if } 30^\circ < \theta < 60^\circ \\ \frac{T_C - T_{sat}}{|\phi_C|} & \text{if } \theta \ge 60^\circ \end{cases} \tag{32}$$

Here, the temperature gradients on both sides of the interface have been determined. Hence, the mass evaporating rate in the macro region can be computed by the following.

$$\int_V \dot{m}_{macro} dV = \frac{1}{\gamma} \int_\Gamma \dot{q} dS \approx \frac{1}{\gamma} \left(\lambda_1 \left(\frac{\partial T}{\partial n}\right)_1 + \lambda_2 \left(\frac{\partial T}{\partial n}\right)_2\right) \Delta l \tag{33}$$

in which, Δl is the length of the interface piece inside cell (i, j).

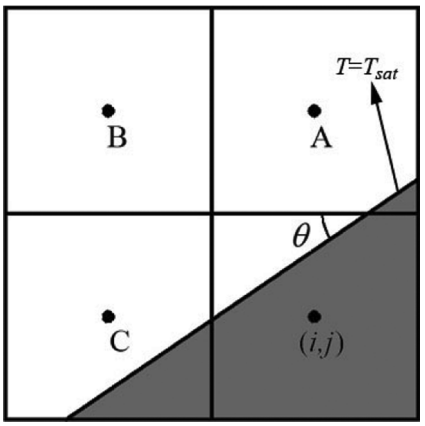

Figure 6. Computing temperature gradient on other side.

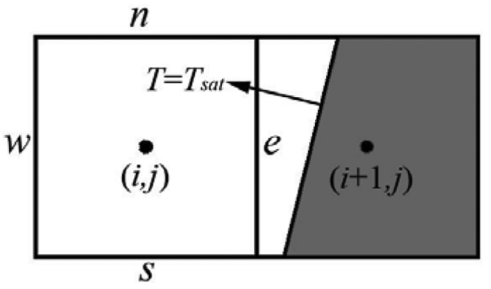

Figure 7. A special case for determination of temperature and its gradient.

Special attention should be paid to the determination of the temperature gradient for those second type cells with neighboring cells whose centers are in the other phase, as shown in Figure 7. For the east interface temperature of cell (i, j) and its temperature gradient, the following equations are suggested based on the fact that the interface between the two cell centers is a better condition for interpolating with closer distance and more accurate temperature ($T = T_{sat}$).

$$T_e \approx \frac{0.5hT_{sat} + (d - 0.5h)T_{i,j}}{d}, \quad \left(\frac{\partial T}{\partial x}\right)_e \approx \frac{T_{i+1,j} - T_{sat}}{d} \tag{34}$$

in which, $d = \frac{|\phi_{i,j}|}{|\phi_{i,j}| + |\phi_{i+1,j}|} h$, where h is the grid length step.

4. RESULTS AND DISCUSSION

The active nucleation sites density is an important parameter in nucleate boiling. For including the effect of active sites density, the method proposed in reference [15] is adopted. In this method, the active sites are assumed to be distributed on the wall averagely and the computation domain size can be decided by the given active site density (Figure 8). In our study, the active site density is set to be $n = 10{,}000\,\mathrm{m}^{-2}$. Under this condition, an active site occupies a square on the heating wall surface with side length of 1 cm in average. In 2-D simulation, a wall length of 1 cm in x-direction contains one nucleation site. In the present study, single-bubble model (Figure 9*a*) is calculated first. For considering more complicated situations, two calculations in other cases are performed. In the one, two bubbles rise at different paces (Figure 9*b*). In the other case, two active sites are close to each other and the two bubbles born in the two sites merge before departing (Figure 9*c*). Computational domain can be halved according to symmetry (marked in gray). In all cases, the initial bubble nucleus is placed on the wall by setting the value of VOF function in the cell touching the nucleation site to 0.5; therefore, the size of the bubble nucleus is smaller than a cell. The waiting time referring to the time between departure of a bubble and formation of the following bubble is set to be 5 ms and the initial

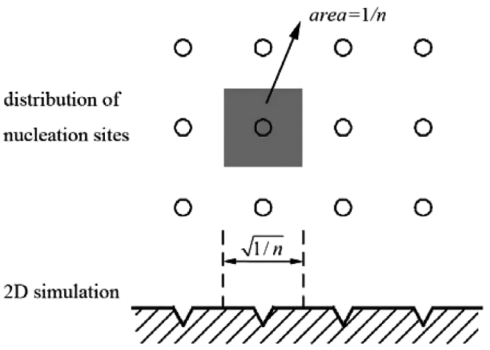

Figure 8. Method for including effect of nucleation sites density.

temperature field is assumed as follows.

$$T = T_{sat} + (T_w - T_{sat}) \exp\left(\frac{-y}{1.25 \times 10^{-4}}\right) \tag{35}$$

where y refers to the distance between cell center and the heating wall.

4.1. Single Bubble Rising

Grid independence is tested before computation. Figure 10 displays the interface at $t = 60$ ms computed under three different mesh sizes. It shows that the mesh size of $h = 1/4$ mm is too large, but little difference can be found between $h = 1/8$ mm and $h = 1/16$ mm. Therefore, mesh size of $h = 1/8$ mm is used for our simulation.

Figure 11 shows the behavior of a bubble in one cycle. An initial bubble nucleus is set on the wall. The bubble grows by evaporation under both effects of surface tension and buoyancy. In the first stage of the bubble's growth when the bubble volume is small, surface tension dominates and the bubble base expands along the wall for increasing of the bubble volume. As the bubble volume becomes large enough and the buoyancy dominates, the bubble base shrinks until the interface completely separates with the wall, leading to departure of the bubble.

Figure 12 shows liquid-vapor interface, flow field and surplus temperature ($T_w - T_{sat}$) during the process of departure and rising of the first bubble. From the figures following features may be noted. First, both liquid and vapor phases on the

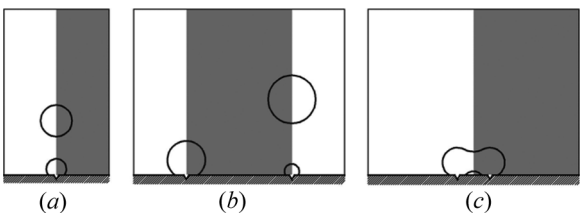

Figure 9. Models to be simulated. (*a*) Single bubble model; (*b*) two bubbles model; and (*c*) bubbles merger model. (Computational domains are marked in gray.)

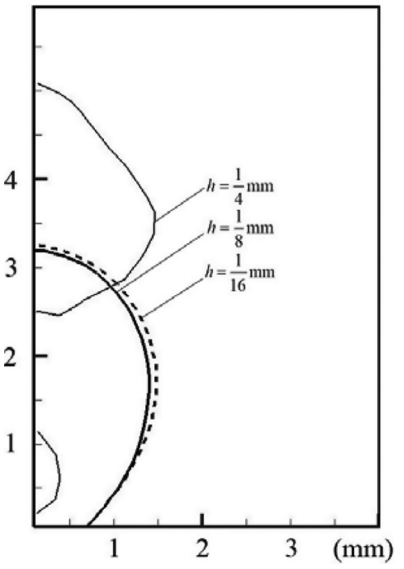

Figure 10. Result of grid independence test.

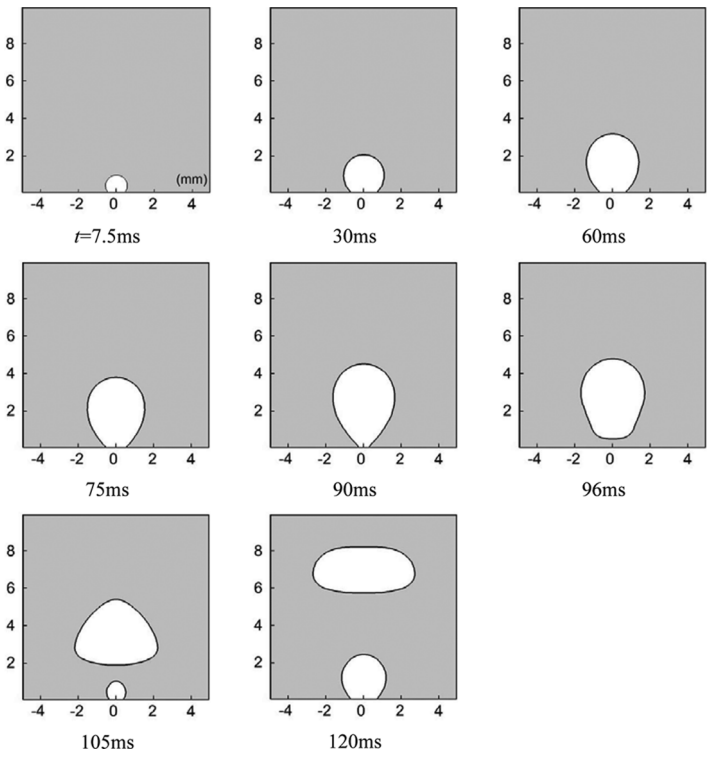

Figure 11. Interface evolution of single bubble model.

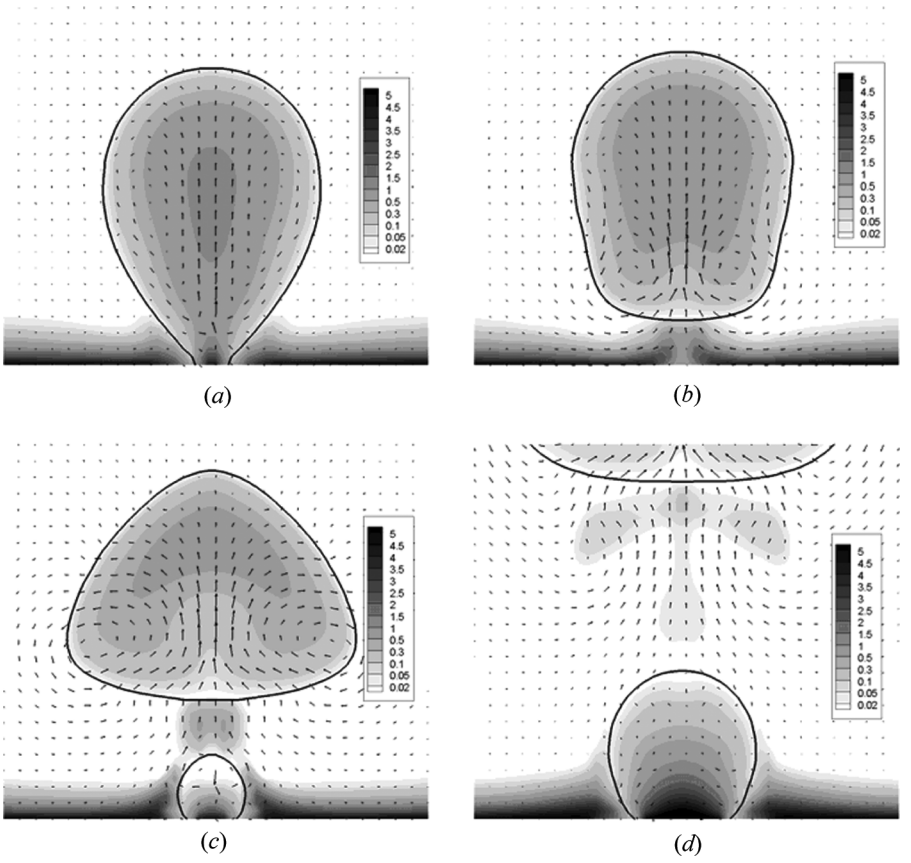

Figure 12. Surplus temperature field and velocity field during bubble departure and rising. (*a*) $t = 91.5$ ms, (*b*) $t = 97.5$ ms, (*c*) $t = 105$ ms, and (*d*) $t = 132$ ms.

two sides of interface are superheated. It is successfully simulated by the temperature interpolation method presented here, and at least qualitatively better than those results with the assumption of constant vapor temperature. Second, as the bubble departs from the wall (Figure 12*b*), two vortexes are formed on the rear of the bubble. By effect of the vortexes, superheated liquid flows to the bubble's rear and the original position is occupied by cold liquid flowing from bulk region. Thus the superheated liquid layer around the wall becomes thinner. Third, as the bubble rises, vortexes grow larger and more hot liquid vicinity to the wall is removed, then a new small bubble occurs (Figure 12*c*). Fourth, as the bubble rises to a certain height so that the effect of the vortexes to the wall becomes smaller (Figure 12*d*), fewer hot liquid is removed. At this moment, a mushroom-shaped overheated liquid area is formed in the rear position of the rising bubble. In this process, large amount of heat stored in superheated liquid in the vicinity of the wall is removed. The result agrees with the transient conduction model for nucleate boiling [5].

According to the mechanism of nucleate boiling, the space-average heat flux contains micro portion and macro portion. The micro portion refers to heat

conduction in the micro region and the macro portion refers to heat conduction and advection in the macro layer. Both portions are averaged along the wall.

$$q = q_{micro} + q_{macro} \tag{36}$$

In which, q_{micro} has been obtained by Eq. (14). The space-average heat flux of macro portion can be computed by temperature gradient on the wall.

$$q_{macro} = \frac{1}{L}\int_0^L \lambda(x)\frac{\partial T}{\partial y}\bigg|_{y=0} dx \tag{37}$$

The local thermal conductivity is computed by the following.

$$\lambda(x) = c\lambda_v + (1-c)\lambda_l \tag{38}$$

Unless stated otherwise, heat flux mentioned below refers to the space-average heat flux.

Figure 13 illustrates the heat flux in the macro region computed by Eq. (37). In the single-bubble model, calculation is being carried on until the third bubble departs from the wall. The initial high value of q_{macro} is caused by the preset initial temperature field, and it declines as liquid is heated. When the first bubble departs from the wall, as analyzed above, large amount of heat is removed from the wall, so a clear increase of q_{macro} occurs (from 0.09 s to 0.1 s). The other two significant increases of q_{macro} correspond to the subsequent two bubbles' departure.

It should be noted that in the period from departure of a first bubble to formation of the second bubble, i.e., the waiting period, the heating surface is covered completely by liquid in macro region, and heat transfer in the micro region disappears,

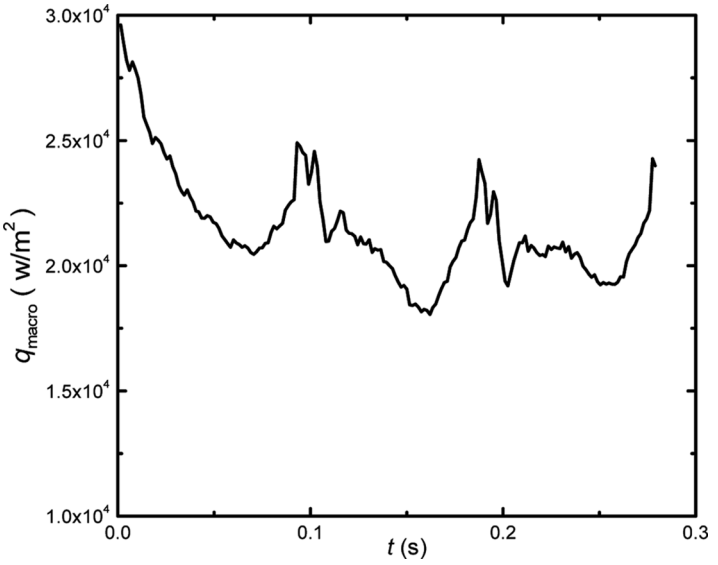

Figure 13. Heat flux versus time in macro region of single bubble model.

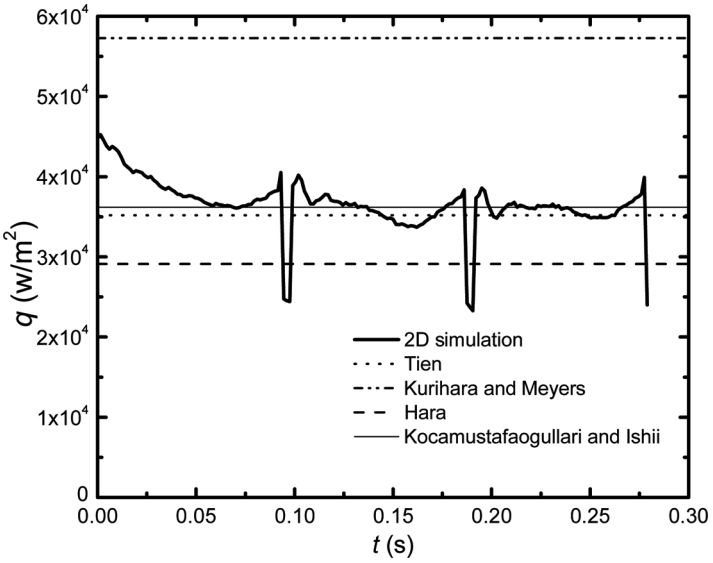

Figure 14. Heat flux versus time of single bubble model and comparison with experimental correlations.

hence, the total heat flux decreases. Figure 14 shows the total heat flux including heat flux in micro region. The three troughs correspond to the three waiting periods after bubbles' departure.

Some experimental correlations that include nucleate site density explicitly [29–32] are list in Table 2. Heat fluxes are computed by these correlations under the same conditions. They are also plotted in Figure 14. As displayed there, the heat flux by simulation is generally among values computed by experimental correlations. Especially, the heat flux by our simulation is very close to Tien and Kocamustafaogullari's correlation, with an average deviation of 4% and 1.2%, respectively.

4.2. Two Bubbles Rising in Different Paces

In the single-bubble model, an implied assumption is made that all bubbles forms at the same time. However, in most instances, bubbles form at different times. As a model closer to actual situation, a two-bubble model is studied in which one

Table 2. Experimental correlations for nucleate boiling

Author	Correlation
Tien [29]	$q = 61.3\mathrm{Pr}_l^{0.33}\lambda_l \Delta T n^{1/2}$
Hara [30]	$q = (C_1C_2)^{3/4}(4\pi C_2/3)^{-1/2}(\rho_l c_{p,\,l}\lambda_l)^{3/4}(\rho_v\gamma)^{-1/2}\Delta T^{3/2}n^{3/8}$ $C_1 = 5.5,\ C_2 = 0.056$
Kurihara and Meyers [31]	$q = 36\lambda_l \mathrm{Pr}_l^{0.33}(\rho_v/\mu_l)^{1/3}\Delta T n^{1/3}$
Kocamustafaogullari and Ishii [32]	$q = 14\lambda_l(\rho_l c_{p,\,l}/\rho_v\gamma)^{1/2}\mathrm{Pr}_l^{-0.39}[0.012((\rho_l-\rho_v)/\rho_v)^{0.9}D_{bF}]^{-0.25}\Delta T^{1.5}n^{3/8}$ $D_{bF} = 0.0208\phi\sqrt{\frac{\sigma}{g(\rho_l-\rho_v)}}$

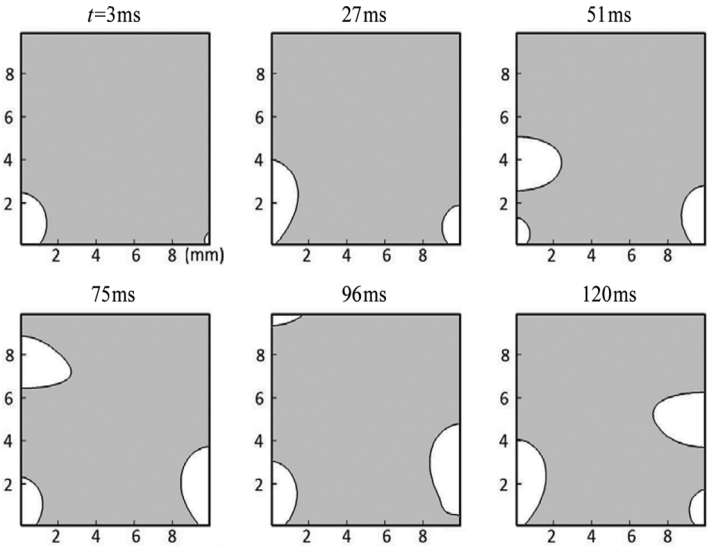

Figure 15. Interface evolution of two-bubble model.

bubble's formation, growth and departure is earlier than the other (shown in Figure 9*b*). The bubble on the left is set with initial radius of 1 mm while only a bubble nucleus is set on the right. In this case, the computation domain should be doubled compared with single-bubble model.

The interface evolution from initial to departure of the two bubbles is illustrated in Figure 15. As the first bubble on the left departs, the right bubble is in growth period. As the right bubble departs, the second bubble on the left has formed and it is growing. In the two nucleation sites, bubbles form and depart alternately. In this

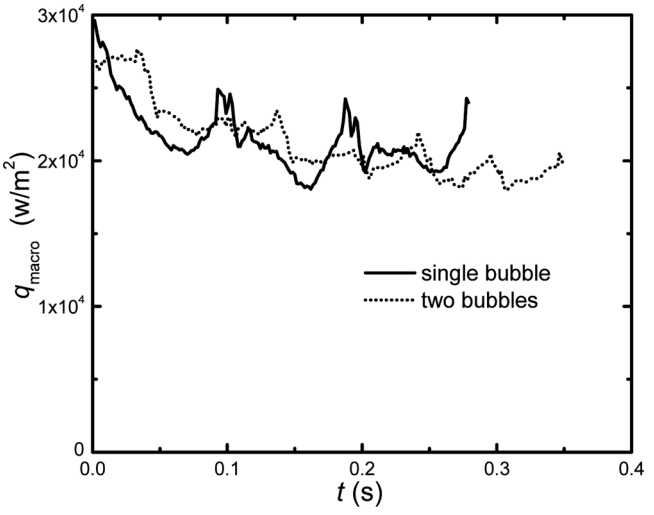

Figure 16. Heat flux versus time in macro region of two-bubble model.

case, calculation is being carried on until the fourth bubble on the left departs. Therefore, in the simulation period seven bubbles in all have departed.

The average heat flux in the macro region is displayed in Figure 16 along with comparison with single-bubble model. As the same with single-bubble model, a bubble's departure can cause a temporary increase in heat flux, therefore seven peaks can be found in the curve. In general, the bubble size at departure and average heat transfer in macro region change little compared with single-bubble model.

4.3. Two Bubbles Merging

In nucleate boiling, nucleate sites are distributed on superheated wall surface randomly and usually unevenly [1]. Therefore, there will be the situation that the

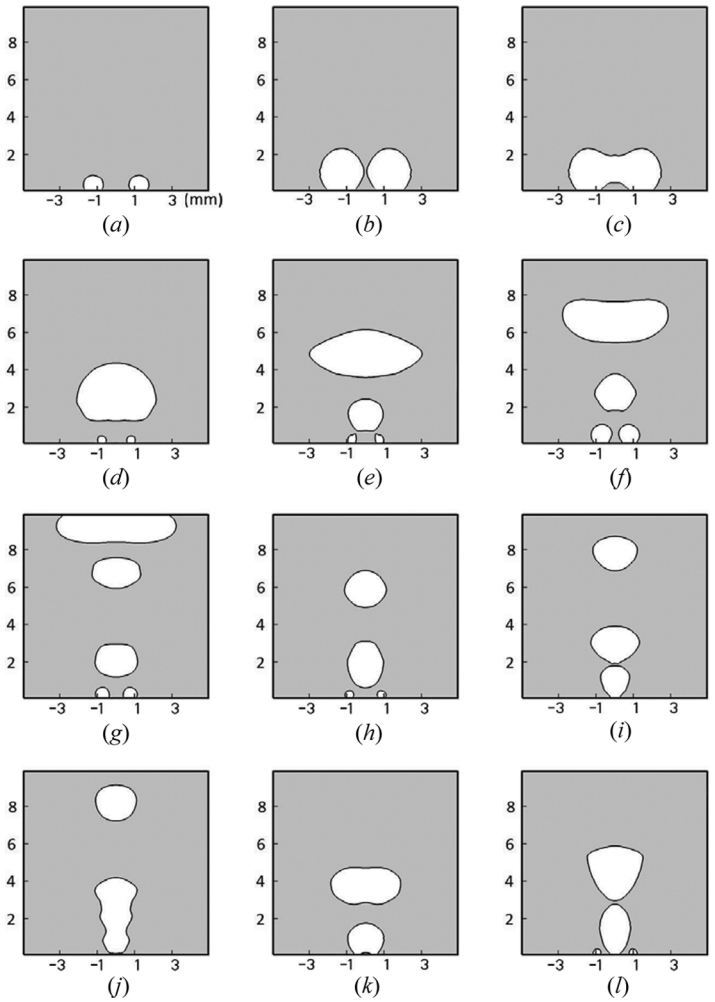

Figure 17. Interface evolution of two bubbles merger model. (*a*) 7.5 ms, (*b*) 28.5 ms, (*c*) 30 ms, (*d*) 45 ms, (*e*) 61.5 ms, (*f*) 75 ms, (*g*) 90 ms, (*h*) 109.5 ms, (*i*) 118.5 ms, (*j*) 120 ms, (*k*) 135 ms, and (*l*) 141 ms.

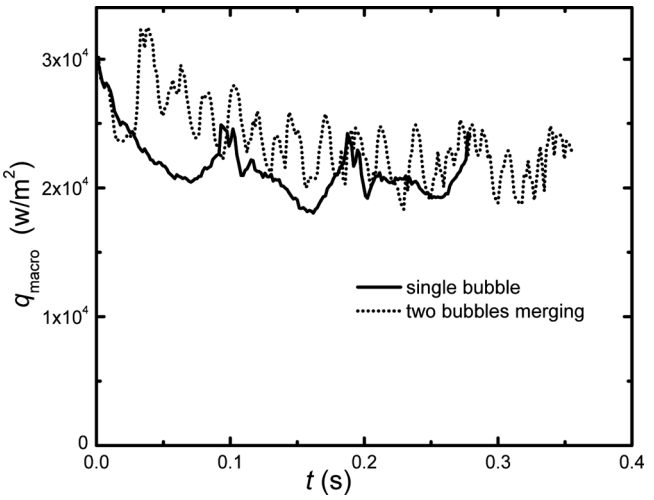

Figure 18. Heat flux versus time in macro region of two bubbles merger model.

distance between two nucleate sites are very close to each other. If the distance is small enough, the two bubbles from the two sites will merge when growing. It can be expected that in this situation, bubbles will act in a much different way. Therefore, the particular case is simulated by changing the positions of nucleation site. The computation domain for this case is displayed in Figure 9*c* and the two nucleation sites are 2 mm from each other. Other conditions are kept unchanged.

Evolution of liquid-vapor interface is displayed in Figure 17. In this case, behavior of bubbles becomes much more complicated. As the two bubbles born in two nucleation sites grow to enough sizes that they can touch each other, by effect of surface tension, the two small bubbles merge and form a new, larger bubble within short time. In this process, a small liquid drop is entrapped below (Figure 17*c*). Thereafter, the merged bubble departs from the wall quickly. The bubble that has just departed usually absorbs several newly formed bubble nucleus and grows larger (Figure 17*e*). In some cases, departed bubble can re-contact with the wall (Figures 17*i* and 17*l*). It is also observed that some merged bubbles can merge vertically, with bubbles that has departed previously (Figure 17*j*). In general, because influenced by the merging process, bubbles depart much more frequently from the wall.

The average heat flux in macro region is illustrated in Figure 18 in dotted line. Because of more frequent bubble departure, more peaks can be found in this curve. Furthermore, heat flux in macro region is increased in contrast with single-bubble model.

CONCLUSIONS

1. The processes of bubble growing, departure, rising, and merging in nucleate boiling are simulated successfully by VOSET method. For including the effect of thin liquid layer around three-phase contact point, a multiscale system method is used by dividing the computation domain into micro and macro regions. Heat flux in

the micro region is computed first and the results are provided as input conditions for solving the macro region.
2. For solving the temperature field in nucleate boiling where both phases are superheated, a temperature interpolation method is proposed. By this method, theoretically expected temperature field is obtained for the vapor phase, which is better than, at least qualitatively, those with the popular used assumption that the temperature of vapor phase is constant and equal to the saturated temperature.
3. Some mechanisms for nucleate boiling are verified by our simulation. In the microlayer, very large value of local heat flux is found. As a bubble departs and rises, superheated liquid is removed away from the wall by vortexes in the rear of the bubble. The heat flux predicted in our simulation agrees well with published experimental correlation.
4. The effect of interaction between the two bubbles is small under the condition used in two-bubble model. But if two bubbles merge in growth period, the heat flux can be increased.

FUNDING

This study was supported by the Key Project of National Natural Science Foundation of China (51136004) and the National Basic Research Program of China (973 Program) (2013CB228304).

REFERENCES

1. J. H. Lienhard, Things We Don't Know About Boiling Heat Transfer, *Int. Comm. in Heat Mass Transfer*, vol. 15, pp. 401–428, 1988.
2. Y. L. He and W. Q. Tao, Multiscale Simulations of Heat Transfer and Fluid Flow Problems, *ASME J. of Heat Transfer*, vol. 134, pp. 031018, 2012.
3. N. Kurul and M. Z. Podowski, Multidimensional Effects in Forced Convection Subcooled Boiling, *Proc. of the 9th Int. Heat Transfer Conf.*, pp. 21–26, 1990.
4. G. Son, V. K. Dhir, and N. Ramanujapu, Dynamics and Heat Transfer Associated with a Single Bubble during Nucleate Boiling on a Horizontal Surface, *ASME J. of Heat Transfer*, vol. 121, pp. 623–631, 1999.
5. J. Kim, Review of Nucleate Pool Boiling Bubble Heat Transfer Mechanisms, *Int. J. Multiphase Flow*, vol. 35, pp. 1067–1076, 2009.
6. D. A. Labuntzov, Heat Exchange at Boiling of Liquids, *Thermal Energy Engineering*, vol. 12, pp. 19–26, 1959. (In Russian.)
7. M. Shoji, Boiling Chaos and Modeling, *Proc. of 11th Int. Heat Transfer Conf.*, vol. 1, pp. 3–21, 1998.
8. C. W. Hirt and B. D. Nichols, Volume of Fluid (VOF) Method for the Dynamcis of Free Boundary, *J. Computational Physics*, vol. 39, pp. 201–225, 1981.
9. S. Osher and J. A. Sethian, Fronts Propagating with Curvature Dependent Speed: Algorithms Based on Hamilton-Jacobi Formulations, *J. Computational Physics*, vol. 79, pp. 12–49, 1988.
10. D. L. Sun and W. Q. Tao, A Coupled Volume-of-Fluid and Level Set (VOSET) Method for Computing Incompressible Two-Phase Flows, *Int. J. Heat and Mass Transfer*, vol. 53, pp. 645–655, 2010.
11. H. Y. Yoon, S. Koshizuka, and Y. Oka, Direct Calculation of Bubble Growth, Departure, and Rise in Nucleate Pool Boiling, *Int. J. Multiphase Flow*, vol. 27, pp. 277–298, 2001.

12. G. Son, N. Ramanujapu, and V. K. Dhir, Numerical Simulation of Bubble Merger Process on a Single Nucleation Site During Pool Nucleate Boiling, *ASME J. of Heat Transfer*, vol. 124, pp. 51–62, 2002.
13. G. Son and V. K. Dhir, Numerical Simulation of Nucleate Boiling on a Horizontal Surface at High Heat Fluxes, *Int. J. Heat and Mass Transfer*, vol. 51, pp. 2566–2582, 2008.
14. Y. Nam, E. Aktinol, V. K. Dhir, and Y. S. Ju, Single Bubble Dynamics on a Superhydrophilic Surface with Artificial Nucleation Sites, *Int. J. Heat and Mass Transfer*, vol. 54, pp. 1572–1577, 2011.
15. S. Shin, S. I. Abdel-Khalik, and D. Juric, Direct Three-Dimensional Numerical Simulation of Nucleate Boiling using the Level Contour Reconstruction Method, *Int. J. Multiphase Flow*, vol. 31, pp. 1231–1242, 2005.
16. A. Mukherjee and V. K. Dhir, Study of Lateral Merger of Vapor Bubbles During Nucleate Pool Boiling, *ASME J. of Heat Transfer*, vol. 126, pp. 1023–1039, 2004.
17. A. Mukherjee and S. G. Kandlikar, Numerical Study of Single Bubbles with Dynamic Contact Angle During Nucleate Pool Boiling, *Int. J. Heat and Mass Transfer*, vol. 50, pp. 127–138, 2007.
18. E. Aktinol and V. K. Dhir, Numerical Simulation of Nucleate Boiling Phenomenon Coupled with Thermal Response of the Solid, *Microgravity Sci. Tech.*, vol. 24, pp. 255–265, 2012.
19. H. B. Ma, P. Cheng, B. Borgmeyer and Y. X. Wang, Fluid Flow and Heat Transfer in the Evaporating Thin Film Region, *Microfluid Nanofluid*, vol. 4, pp. 237–243, 2008.
20. S. V. Patankar, *Numerical Heat Transfer and Fluid Flow*, McGraw-Hill, New York, 1980.
21. W. Q. Tao, *Numerical Heat Transfer*, 2nd ed., Xi'an Jiaotong University Press, Xi'an, P.R. China, 2001.
22. G. Tryggvason, R. Scardovelli, and S. Zaleski, *Direct Numerical Simulations of Gas-Liquid Multiphase Flows*, Cambridge University Press, New York, NY, 2011.
23. J. U. Brackbill, D. B. Kothe, and C. Zemach, A Continuum Method for Modeling Surface Tension, *J. Computational Physics*, vol. 100, pp. 335–354, 1992.
24. S. Afkhami and M. Bussmann, Height Functions for Applying Contact Angles to 2-D VOF Simulations, *Int. J. Numer. Methods in Fluids*, vol. 57, pp. 453–472, 2008.
25. B. V. Leer, Towards the Ultimate Conservative Difference Scheme, V. A Second-Order Sequel to Gudnov's Method, *J. Computational Physics*, vol. 23, pp. 101–136, 1977.
26. W. Q. Tao, *Recent Advances in Computational Heat Transfer*, pp. 125–139, Science Press, Beijing, P.R. China, 2000.
27. D. Z. Guo, Research of Two-Dimensional Horizontal Film Boiling based on VOSET Method, Thesis for Master's Degree, Xi'an Jiaotong University, Xi'an, P.R. China, 2010.
28. D. Z. Guo, D. L. Sun, Z. Y. Li, and W. Q. Tao, Phase Change Heat Transfer Simulation for Boiling Bubbles Arising from a Vapor Film by VOSET Method, *Numer. Heat Transfer A*, vol. 59, pp. 857–881, 2011.
29. C. L. Tien, A Hydrodynamic Model for Nucleate Pool Boiling, *Int. J. Heat and Mass Transfer*, vol. 5, pp. 533–540, 1962.
30. A. Hara, The Mechanism of Nucleate Boiling Heat Transfer, *Int. J. Heat and Mass Transfer*, vol. 6, pp. 959–969, 1963.
31. H. Kurihara and J. E. Myers, The Effects of Superheat and Surface Roughness on Boiling Coefficients, *AIChE J.*, vol. 6, pp. 83–91, 1960.
32. G. Kocamustafaogullari and M. Ishii, Interfacial Area and Nucleation Site Density in Boiling System, *Int. J. Heat and Mass Transfer*, vol. 26, pp. 1377–1387, 1983.